JACS
JOURNAL OF THE AMERICAN CHEMICAL SOCIETY

ARTICLE

pubs.acs.org/JACS

Synthesis and Catalytic Properties of Nanoparticulate Intermetallic Ga−Pd Compounds

Marc Armbrüster,*[,†] Gregor Wowsnick,[†] Matthias Friedrich,[†] Marc Heggen,[‡] and Raul Cardoso-Gil[†]

[†]Max-Planck-Institut für Chemische Physik fester Stoffe, Nöthnitzer Strasse 40, 01187 Dresden, Germany

[‡]Institut für Festkörperforschung, Forschungszentrum Jülich GmbH, 52425 Jülich, Germany

ABSTRACT: A two-step synthesis for the preparation of single-phase and nanoparticulate GaPd and $GaPd_2$ by coreduction of ionic metal-precursors with $LiHBEt_3$ in THF without additional stabilizers is described. The coreduction leads initially to the formation of Pd nanoparticles followed by a Pd-mediated reduction of Ga^{3+} on their surfaces, requiring an additional annealing step. The majority of the intermetallic particles have diameters of 3 and 7 nm for GaPd and $GaPd_2$, respectively, and unexpected narrow size distributions as determined by disk centrifuge measurements. The nanoparticles have been characterized by XRD, TEM, and chemical analysis to ensure the formation of the intermetallic compounds. Unsupported nanoparticles possess high catalytic activity while maintaining the excellent selectivity of the ground bulk materials in the semihydrogenation of acetylene. The activity could be further increased by depositing the particles on α-Al_2O_3.

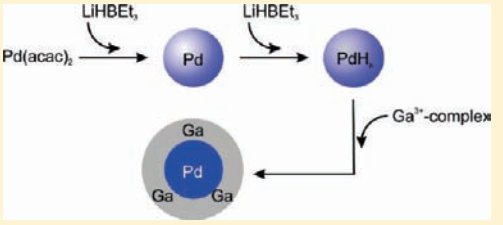

INTRODUCTION

The semihydrogenation of acetylene is an important reaction for the industrial production of polyethylene. Traces of acetylene (~1%) in the ethylene stream produced by naphtha cracking have to be diminished to the low ppm regime since acetylene poisons the polymerization catalyst.[1] Usually Pd or substitutional Ag−Pd alloys[2] supported on α-alumina are applied for the selective hydrogenation of acetylene to ethylene. These catalysts show a high hydrogenation activity but only a limited selectivity to ethylene.[3] In addition, improving the longtime stability is a challenge for future catalytic systems.

The intermetallic compounds $GaPd_2$, GaPd, and Ga_7Pd_3 were found to be excellent catalysts for the selective semihydrogenation of acetylene.[4−6] The ground or milled bulk materials show a high long-term stability and an excellent selectivity to ethylene of 70−78%. This originates from the isolation of the active sites in the crystal structure as well as from the strong alteration of the electronic structure in comparison to elemental Pd. *In situ* XRD, *in situ* EXAFS and *in situ* XPS proved the stability of these compounds under reaction conditions. The aim of these studies was to explore the intrinsic catalytic properties of these well-defined compounds by avoiding additional influences, for example, particle size effects or influences from the support. For this reason, low specific surface areas and hence a low specific activity were tolerated. Industrial systems on the other hand have to make best use of the noble metal. To enhance the catalytic activity of the Ga−Pd intermetallic compounds, we are interested in the synthesis of well-defined nanoparticles of these materials and their catalytic properties for the semihydrogenation of acetylene.

Until now little has been known about successful syntheses of single-phase nanoparticulate intermetallic compounds of Ga. Abraham et al.[7] produced finely divided powder of Mg_2Ga_5 by reduction of $GaCl_3$ with anthracene-activated Mg, and Cokoja et al.[8] obtained Ga_2Cu by reaction of a copper-mesitylene complex with quinuclidine-stabilized GaH_3. The products were characterized by XRD and no information about particle sizes was given. Several groups attempted the synthesis of supported nanoparticles of Ga-based intermetallic compounds by reductive treatment of Ga_2O_3-supported transition metals like Pd or Co. Precursors of the metals were reduced in a hydrogen-atmosphere at elevated temperatures leading to a reductive metal−support interaction (RMSI) and the subsequent formation of intermetallic compounds.[9−11] These approaches resulted in mixtures of different phases, often still containing elemental transition metals.

For the synthesis of unsupported nanoparticulate intermetallic compounds either laser ablation[12] or solution-based synthesis procedures may be applied. A common solution-based method to generate metallic nanoparticles is the (co)reduction of metal-salts in an organic solvent with a suitable reducing agent, for example, hydrogen or borohydrides. Sometimes the solvent is used simultaneously as a reducing agent like in the case of ethylene glycol or tetraethylene glycol. It was shown in particular by Schaak that the use of high boiling alcohols, known as "polyol process", as mild reducing agents allows the preparation of a wide range of intermetallic compounds.[13−15] In the case of bimetallic nanoparticles containing a metal with an unfavorable reduction potential for the polyol process, for example, Al or Zn, thermal decomposition reactions, hydrogenolysis or combinations of decomposition and hydrogenolysis of adequate metal−organic precursors can be applied.[8,16,17]

The challenge in the preparation of intermetallic Ga−Pd compounds is the difference in redox potentials of Ga^{3+} and

Received: March 29, 2011
Published: May 09, 2011

Pd^{2+}. This complicates a conucleation, which is usually desired for synthesis of bimetallic nanoparticles. The strong Lewis acidity of Ga^{3+}-salts, which tend to form stable complexes with electron donors, also hinders the reduction of Ga^{3+}. In the case of Ga, the situation is even more difficult in comparison to other hard-to-reduce metals because the low melting point of 29.77 °C[18] of elemental Ga impedes a controlled synthesis of nanostructured Ga-materials, due to the high tendency to coagulation of the liquid metal.

Recently, a procedure for the synthesis of intermetallic Cu−Pd nanoparticles was developed.[19] In the following we describe the adoption of this process resulting in a two-step synthetic route giving access to nanoparticulate $GaPd_2$ and GaPd using $LiHBEt_3$ in THF (Superhydride) as reducing agent. Emphasis is placed on the absence of elemental Pd as well as surfactants, which would block or modify the catalytically active surface.[17] Another requirement is the absence of byproducts in the samples, which could modify the catalytic properties in the semihydrogenation of acetylene. Since the development of a reproducible synthesis including the mentioned requirements is not straightforward, special care was taken to also investigate mechanistic aspects of the synthesis. The syntheses described below were developed for unsupported single-phase materials. Modifying the synthesis protocol also allowed the preparation of particles deposited on α-Al_2O_3.

EXPERIMENTAL SECTION

The following reagents were used: $GaCl_3$ (ultra dry, 99.999%, Aldrich), $Pd(acac)_2$ (acac = acetylacetonate, purum, Fluka), $LiHBEt_3$ (Superhydride, 1 M in tetrahydrofuran (THF), Aldrich), $NaBH_4$ (ABCR, powder 98%), Pd/Al_2O_3 (5 wt.%, Aldrich), Pd (ChemPur, 99.95%), Ga (ChemPur, 99.99%), BN (hexagonal, 99.95%, 325 mesh, Aldrich), THF (99.9%, Roth), acetone (Overlack, 99.7%) and dioctylether (99%, Aldrich). Solvents, except acetone, were distilled over CaH_2 under argon before use to remove water and oxygen. Other chemicals were used without further purification. All procedures were carried out under protective argon atmosphere in a glovebox with oxygen and water concentrations below 0.1 ppm. Bulk samples of GaPd and $GaPd_2$ were prepared by melting stoichiometric amounts of the elements under Ar in a high-frequency furnace and subsequent annealing in vacuum as described earlier.[5]

For the investigation of the formation of the nanoparticles, $LiHBEt_3$ in THF was also transferred to dioctylether. Fifteen milliliters of Superhydride were filled in a 3-neck round-bottom flask and 15 mL of dioctylether were added. The solution was allowed to stir for 1.5 h at 1 mbar at 90 °C to remove THF from the mixture. The final solution had a volume of 16.5 mL, indicating that some THF was still present. After adding 0.3 g (1.704 mmol) of $GaCl_3$ to 5.5 mL of $LiHBEt_3$ in dioctylether, a white precipitate of LiCl was formed immediately, followed by an exothermic reaction under formation of gray elemental liquid Ga, which coated the glass wall easily. The suspension was separated by centrifugation (EBA 20, Hettich), washed four times with THF to remove the LiCl and dried at 1 mbar for 20 min to result in 35 mg of elemental Ga.

For the synthesis of nanoparticulate $GaPd_2$, 0.1384 g (0.454 mmol) of $Pd(acac)_2$ were solved in 15 mL THF in a 100 mL 3-neck round-bottom flask. The yellow clear solution was heated to reflux temperature while stirring; 0.1000 g (0.568 mmol) $GaCl_3$ were added to 5.1 mL Superhydride in a separate vessel accompanied by an exothermic reaction leading to a colorless clear solution. This solution was filled in a syringe, placed in a perfusor and connected to the 3-neck flask by a cannula through a septum and pumped with 150 mL/h to the refluxing THF solution, resulting in a black suspension instantly. The suspension was stirred for further 4 h under reflux and subsequently separated by centrifugation at 6000 rpm. The black precipitate was washed three times with THF and dried in dynamic vacuum at 100 mbar for 20 min. The dried particles were resuspended in dioctylether, heated to 185 °C and stirred for another 4 h. After the suspension was centrifuged at 6000 rpm to separate the solid from the liquid, the black precipitate was washed with THF three times to remove the high-boiling dioctylether and dried for 20 min at 100 mbar in dynamic vacuum.

GaPd was synthesized by dissolving 0.1386 g (0.455 mmol) $Pd(acac)_2$ in 15 mL THF in a 100 mL 3-neck round-bottom flask and stirring at ambient temperature; 0.107 g (0.608 mmol) of $GaCl_3$ were added to 5.1 mL Superhydride, filled in a syringe, placed in a perfusor and connected to the 3-neck flask as described above. In contrast to the synthesis of $GaPd_2$, the $GaCl_3$ solution was added to the THF solution with 150 mL/h at *room temperature* resulting in a black suspension instantly. The black suspension was subsequently heated to reflux and stirred for 4 h. The obtained products were separated, cleaned and thermally treated in dioctylether as described above.

For the synthesis of supported particles, coreduction was performed following the above protocols. After washing the particles, they were resuspended in 10 mL THF. Two milliliters of this suspension were filled in a 200 mL 2-neck round-bottom flask filled with 21 g of α-Al_2O_3 as support (20 mL bulk volume, cylindrical pellets treated with 40 mL acetone, subsequently shaken to replace Al_2O_3 powder, then dried at 80 °C for 2 h and at last moistened with 10 mL THF before use). During careful shaking, the THF was slowly evaporated by applying vacuum (150 mbar), which was slowly decreased to 20 mbar during 20 min allowing a slow and homogeneous deposition of the particles on the Al_2O_3. The catalysts were then dried at 1 mbar for 2 h. Subsequently, 50 mL of dioctylether were added and the deposited particles were treated in suspension at 250 °C for 4 h. The dioctylether was decanted and the catalyst was washed four times with 50 mL of THF under careful shaking, causing some loss of particles due to the mechanical treatment. In the last step, the pellets were dried at 1 mbar for 2 h.

X-ray powder diffraction (XRD) was performed on an image plate Guinier camera (Huber G670, Cu−Kα_1 radiation, λ = 1.54056 Å, quartz monochromator, $3° \leq 2\theta \leq 100°$). To prevent contact with air, the powders were mounted between two 7.5 μm Kapton foils. Temperature-dependent X-ray powder diffraction was performed on a STOE-STA-DIP-MP diffractometer (Cu−Kα_1 radiation, λ = 1.54056 Å, Ge-monochromator) using a high-temperature setup and placing the samples in Ar-filled quartz glass capillaries.

TEM images were taken at a Tecnai 10 (LaB_6 cathode) at 100 kV. High-resolution TEM images were taken at a spherical-aberration corrected FEI TITAN 80−300 transmission electron microscope operated at 300 kV. Negative spherical aberration imaging (NCSI) was used, providing optimum bright atom contrast up to the information limit.[20,21] Samples for TEM analysis were prepared from a methanol suspension on a carbon-coated copper grid (300 mesh, SPI supplies).

Disk centrifuge (DC) measurements on a CPS DC24000 were used to determine the particle size distribution of the unsupported samples. The dried samples were suspended in cyclohexane before being injected into the rotating disk. The disk speed was set to 24 000 rpm and the density gradient was built up from cyclohexane and halocarbon with a density of 1.8 g/cm^3. Elemental compositions of the samples were determined by ICP-OES (Varian, Vista RL). Nanoparticulate samples were dissolved in aqua regia diluted with deionized water and measured applying a commercial standard for calibration. Metal contents of organic solutions were determined using a matrix adjusted standard.

The catalytic measurements were performed in a plug-flow reactor at 473 K; a detailed description of the reaction setup has been given

elsewhere.[5] Deposited samples were crushed and diluted with 150 mg of inert BN. The feed composition was 0.5% acetylene (solvent free, 99.5%, 5% in He, 99.999%), 5% hydrogen (99.999%), 50% ethylene (99.95%) in helium (99.999%), and the total flow was 30 mL/min. The gases were supplied by Praxair (C_2H_2, He and H_2) and Westfalen Gas (C_2H_4). The product gas composition was determined by a Varian CP 4900 MicroGC gas chromatograph. Conversion and selectivity to ethylene were calculated as stated in ref 5.

RESULTS AND DISCUSSION

The First Step—Coreduction. The challenge for the synthesis of intermetallic Ga−Pd compounds is to find the optimum reducing conditions for Ga. On the one hand, mild reducing agents are not capable to reduce the Ga^{3+} with its low redox potential and its high Lewis-acidity. On the other hand, a very fast reduction of Ga^{3+} will most probably cause coagulation of the low-melting metal, handicapping the formation of nanoparticulate materials. Because Pd^{2+} is easier to reduce to the elemental state, a coreduction of Pd^{2+} and Ga^{3+} is likely to produce first Pd nanoparticles, which then can act as nucleation centers for the Ga atoms.

Single-phase nanoparticulate $GaPd_2$ and GaPd can indeed be obtained by coreduction of $Pd(acac)_2$ and $GaCl_3$ with $LiHBEt_3$ in THF ("coreduction") and subsequent annealing in dioctylether at high temperatures ("annealing"). In the first step, an excess of $GaCl_3$ is necessary for the formation of GaPd and $GaPd_2$ since the reduction of the Ga precursor is not quantitative and high temperatures and 4 h reaction time with a large excess of Superhydride are required to reduce Ga^{3+}. The reaction parameters are crucial. The success of the coreduction strongly depends on the reduction temperature, the reducing agent and the solvent as well as on the counterion of Ga^{3+}. The initial reduction temperature is important to obtain reproducible single-phase intermetallic GaPd or $GaPd_2$, and experiments revealed that using $NaBH_4$ instead of $LiHBEt_3$ as reducing agent was not powerful enough to reduce the $GaCl_3$ and hence to obtain any intermetallic compounds. Replacing $GaCl_3$ by $Ga(acac)_3$ hindered a successful reduction, even when Superhydride was used as the reducing agent. The strong dependence of the system on the solvent can be seen by changing from THF to dioctylether as solvent for the reduction of $GaCl_3$ in the absence of Pd^{2+}. While no reaction occurs in THF, most likely because of a better stabilization of Ga^{3+} by O-donor bonds, it is possible to reduce Ga^{3+} to the elemental state in dioctylether, using $LiHBEt_3$ as reducing agent in both cases. These observations show that the synthesis does not follow the intuitive reaction equation given below for GaPd:

$$2Pd(acac)_2 + 2GaCl_3 + 10LiHBEt_3 \rightarrow 2GaPd + 4Li(acac) + 6LiCl + 10BEt_3 + 5H_2$$

To gain a deeper understanding of the processes during the coreduction, we fragmented this process into simpler reaction systems and investigated them separately.

Even if the reduction of Pd^{2+} to the elemental state by Superhydride should be straightforward, the details of this reaction will elucidate important findings for the complete synthesis. Superhydride ($LiHBEt_3$ in THF) is a strong reducing agent, powerful enough to reduce even such hard-to-reduce metal ions in metal halogenides like $ZnCl_2$ to result in finely dispersed metal powders.[22] Besides being a solvent, THF acts as stabilizer and inhibits the growth of the particles. As expected, the reduction of $Pd(acac)_2$ to Pd is fast and quantitative at ambient temperature under evolution of H_2. Therefore, the reaction scheme can be written as

$$Pd(acac)_2 + 2LiHBEt_3 \rightarrow Pd + H_2 + 2Li(acac) + 2BEt_3$$

In the presence of unconsumed $LiHBEt_3$, the complex $Et_3BHBEt_3^-$ is formed,[23] which might still be able to reduce Pd^{2+} to the elemental state.

Looking at the second reduction separately, that is, $GaCl_3$ to elemental Ga, an interesting observation is made. If only $GaCl_3$ is reacted with $LiHBEt_3$, no significant amount of Ga is formed, even at reflux temperature. Adding $GaCl_3$ to Superhydride at ambient temperature causes an exothermic reaction and results in a colorless solution. The reason is most probably the high Lewis-acidity of Ga^{3+} and the electron-donor activity of THF leading to stable complexes, for example, $GaCl_3 \cdot THF$,[24] of $GaCl_3$ with this ligand, which are resistant against further reduction. Furthermore, ether cleavages of THF forming Ga−O bonds or the formation of lower valent Ga species, for example, $Ga_2Cl_4(THF)_2$,[25] being themselves strong reducing agents are possible additional reactions. Evidence for the responsibility of the electron donor activity of THF as cause for the difficulty of the reduction can be collected by exchanging THF for dioctylether. In this more unpolar solvent the reduction of $GaCl_3$ by $LiBEtH_3$ takes place immediately. The yield is about 30% but this might be due to residual THF in the mixture (see Experimental section). Although dioctylether seems to lead to higher yields of Ga, such fast reductions do not seem to be suitable for the preparation of nanoparticulate intermetallic Ga compounds since the low melting point of Ga causes a strong coagulation of the liquid metal under these conditions. In addition, $Pd(acac)_2$ being less soluble in dioctylether is the reason why the optimized protocols were performed using THF as solvent.

From these experiments follows that the reduction of Ga^{3+} occurs in THF only in the presence of Pd. The following scenario is suggested: During the coreduction of Pd^{2+} and Ga^{3+}, Pd^{2+} will be reduced immediately and then mediates the reduction of Ga^{3+}. The role of Pd can be understood by considering its ability to activate hydrogen by forming very active Pd hydrides,[26] which in turn reduce the Ga^{3+} to elemental Ga. In addition, this explains the homogeneity of the products as well as why elemental Ga is never observed in the coreduction, since Ga would only be reduced on the surface of the Pd particles and does not form particles of its own.

To summarize these results: A controlled reduction of Ga^{3+} to a nanoparticulate Ga compound in THF is hindered by the high stability of the immediately formed Ga^{3+} complexes. Using an unpolar solvent diminishes the formation of complexes but causes a fast uncontrolled reduction followed by coagulation. The presence of elemental Pd mediates the reduction of Ga^{3+} in

Scheme 1. Proposed Mechanism for the Formation of the Nanoparticulate Ga−Pd Precursor[a]

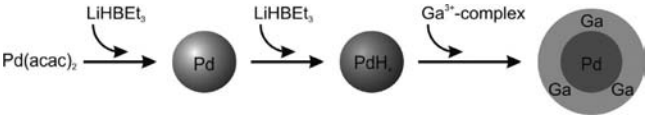

[a] Stable Ga^{3+} complex is reduced by palladium-activated hydrogen. The exclusive formation of Ga on the Pd surface inhibits the coagulation of the elemental Ga.

dx.doi.org/10.1021/ja202869d | J. Am. Chem. Soc. 2011, 133, 9112–9118

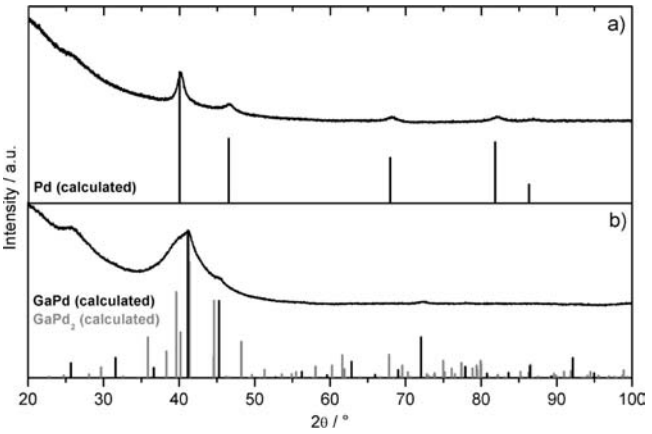

Figure 1. X-ray diffraction patterns of the products of the coreduction for (a) $GaPd_2$ and (b) GaPd after the first reaction step. Calculated patterns are shown in the lower parts of the panels.

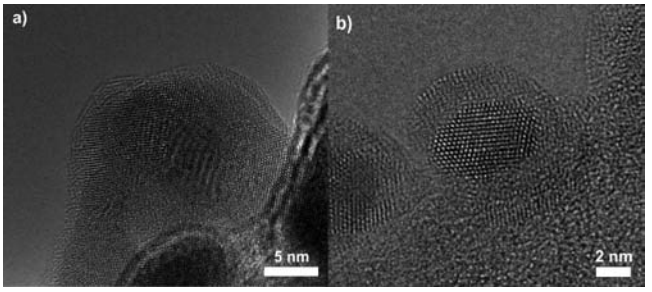

Figure 2. Aberration-corrected HR-TEM of nanoparticles after the coreduction step during preparation of (a) $GaPd_2$ and (b) GaPd. Crystalline particles are surrounded by an additional layer consisting of elemental Ga according to the suggested formation mechanism.

THF by forming active Pd hydrides. From this follows that Ga is formed exclusively on the surface of Pd, thus inhibiting the uncontrolled coagulation (Scheme 1). It also becomes clear why the reaction conditions at the beginning of the reaction, when Pd is formed, are critical for the complex synthesis and determine the products obtained.

After the coreduction, which is the first step in the synthesis, no single-phase intermetallic compounds could be obtained. As discussed in detail in the following, Ga does not ($GaPd_2$ synthesis) or only partially (GaPd synthesis) diffuse from the Pd surface into the Pd particles during the coreduction and the formation of Pd or a mixture of $GaPd_2$ and GaPd, respectively. This, as well as the yield of Ga, is more dependent on the initial reduction temperature rather than the Ga:Pd ratio used. Elemental analysis of the solid phase after the coreduction shows that only 40 mol-% of Ga^{3+} is reduced when $GaPd_2$ should be synthesized, where the initial reduction temperature is 68 °C (reflux temperature); 75 mol-% of Ga are reduced in the case of GaPd, where the initial temperature is 23 °C. Chemical analyses proved in both cases that the missing Ga^{3+} fraction remained in the liquid, which excludes the formation of any gaseous Ga-species. Two reasons may be responsible for the partial reduction of Ga^{3+}: First, it could be caused by the resulting Ga layer on the Pd particles, which hinder the reformation of the Pd hydride. Second, the incomplete reduction could be due to the formation of highly stable Ga complexes (e.g., with acetylacetonate).

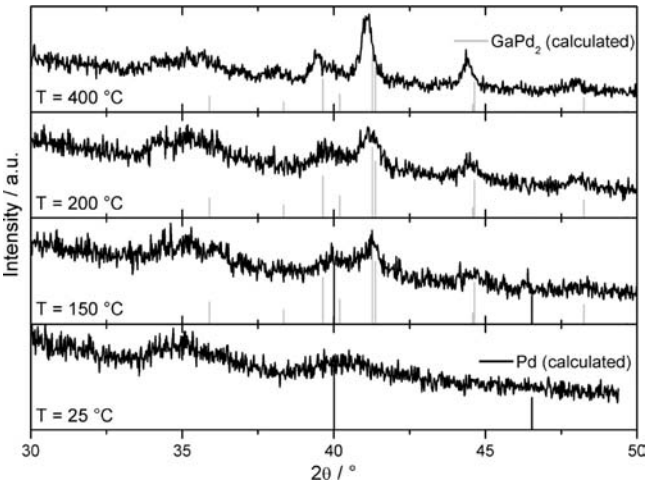

Figure 3. Temperature dependent X-ray diffraction patterns of particles obtained after the coreduction step during the synthesis of $GaPd_2$. The formation of the intermetallic compound $GaPd_2$ starts at around 150 °C. The fwhm of the diffraction lines decreases with increasing temperature due to sintering of the particles.

Figure 1 shows the X-ray powder diffraction data of the products after the first step of the synthesis. The product after the coreduction again depends on the initial reduction temperature. For $GaPd_2$ only nanocrystalline Pd can be observed by X-ray diffraction. In the case u GaPd, a mixture of $GaPd_2$ and GaPd is present. Elemental Ga, liquid due to the low melting point and small size, was not detected by XRD in either case. HR-TEM images (Figure 2) of the particles after the coreduction show small crystalline particles of Pd surrounded by a 2 nm thin layer which most probably consists of Ga, corroborating the suggested formation mechanism. EDX measurements on the particles resulted in a composition of $Pd_{48(1)}Ga_{52(1)}$ and $Pd_{61(1)}Ga_{39(1)}$ for GaPd and $GaPd_2$, respectively.

During the synthesis, special care has to be taken with the drying procedure after the first and the second step. Drying the particles means to remove the stabilizer THF and to cause some unavoidable agglomeration. If the THF is completely removed by applying harsh conditions (e.g., <100 mbar at ambient temperature), the obtained particles will start to sinter spontaneously, leading to a strong energy release, that is, the sample is heated to 300−400 °C. This process was also observed under inert conditions within the glovebox, since the driving force is the minimization of surface energy and not a chemical reaction.

The Second Step—Annealing. As in the case of the Cu−Pd nanoparticles,[19] a treatment at elevated temperatures is necessary to obtain the desired materials. In the present study, annealing in high-boiling dioctylether at 185 °C for 4 h proved to be a suitable procedure to obtain single-phase products. To elucidate the processes in the second step of the synthesis, a powder sample for the preparation of $GaPd_2$ was subjected to temperature dependent X-ray diffraction in Ar atmosphere after the first step. The formation of the intermetallic compound by diffusion of gallium starts around 150 °C (Figure 3). The fwhm of the diffraction lines decreases with increasing temperature due to sintering of the particles. As calculated with the Scherrer equation,[27] the crystallite size of $GaPd_2$ is 10 nm at 150 °C, 12 nm at 200 °C and 25 nm at 400 °C.

dx.doi.org/10.1021/ja202869d |J. Am. Chem. Soc. 2011, 133, 9112–9118

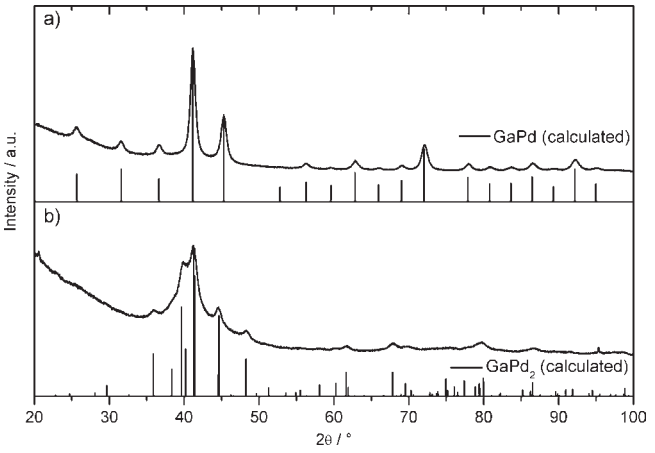

Figure 4. X-ray diffraction patterns of nanoparticulate (a) GaPd and (b) $GaPd_2$ obtained after the second step of the synthesis. Calculated patterns of GaPd and $GaPd_2$ are given for comparison.

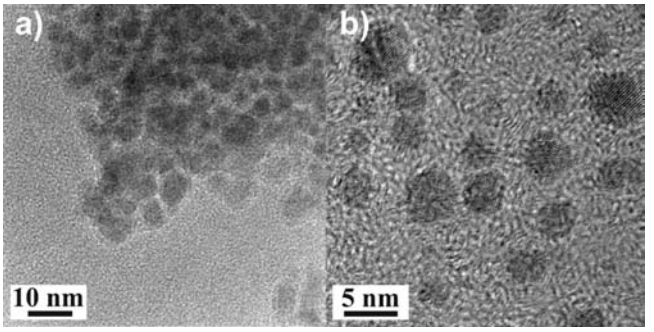

Figure 5. TEM images of the nanoparticles after the annealing step: (a) $GaPd_2$ agglomerate, with primary particles of 3−7 nm; (b) GaPd nanoparticles with diameters of 1−5 nm.

Even if the annealing after the coreduction is performed in suspension, the resulting nanoparticles show a strong agglomeration because the product was dried beforehand and no stable suspensions are formed. The reflections of GaPd in the powder pattern obtained after annealing (see Figure 4) are sharper in comparison with the reflections of $GaPd_2$. A crystallite size of 11 nm was calculated for GaPd and 7 nm for $GaPd_2$, which is smaller than detected during the temperature dependent XRD, probably due to the stabilizing influence of the solvent and the lower temperature. Figure 5 shows TEM images of the dried particles of GaPd and $GaPd_2$. They are nearly spherical and have diameters of around 3−7 nm. Nearly all particles form large agglomerates, which is hardly avoidable because of the absence of additional stabilizers. The surface weighted size distribution relevant for the catalytic properties of the GaPd and $GaPd_2$ nanoparticles was determined by fractional sedimentation in the disk centrifuge after dispersing the primary particles of the agglomerates (Figure 6). The majority of the GaPd nanoparticles possess diameters around 3 nm, but particles with somewhat larger diameters are also present. The discrepancy between the crystallite size of 11 nm and the most abundant particle size of 3 nm can be explained by the small contribution of crystallites <5 nm to the XRD signals. In the case of $GaPd_2$ nanoparticles, the maximum in the size distribution was obtained at 7 nm in accordance with the

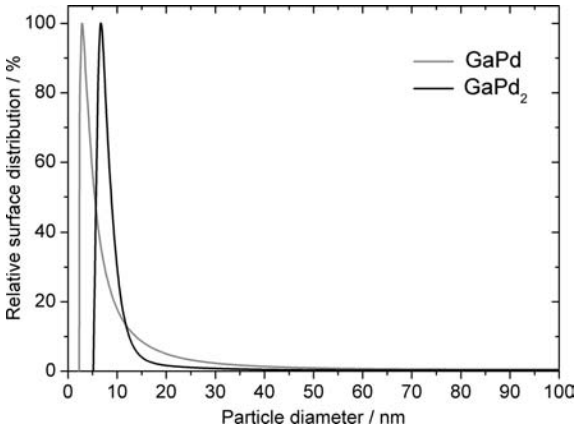

Figure 6. Surface weighted size distribution of $GaPd_2$ and GaPd nanoparticles. $GaPd_2$ nanoparticles have a maximum size at 7 nm and GaPd at 3 nm. The distribution is sharper for $GaPd_2$.

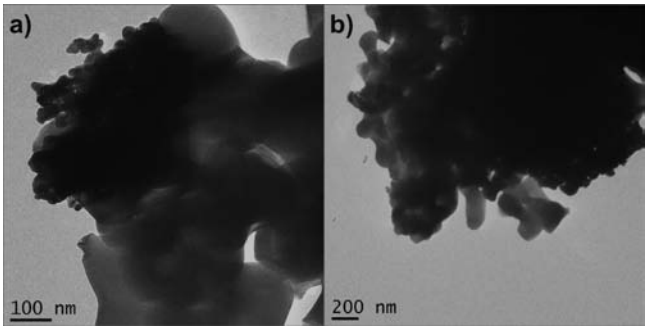

Figure 7. TEM images of (a) $GaPd_2@Al_2O_3$ and (b) $GaPd@Al_2O_3$. The particles are deposited in form of small agglomerates.

XRD results. Considering the absence of stabilizers, the particle size distribution is surprisingly sharp in both cases.

Depositing the Nanoparticles. To further enhance the activity of the catalysts, the particles can be deposited on α-Al_2O_3. In addition, a comparison of the catalytic properties of unsupported and deposited particles allows directly observing influences of the support on the catalytic properties. Since the nanoparticles can be suspended during the first synthesis step (coreduction) and before drying, an easy way to deposit the particles on α-Al_2O_3 is by evaporation of the THF. For this purpose, it is sufficient to wet the support with THF and add a suspension of the nanoparticles. By shaking the pellets during the evaporation of THF, larger agglomerates are broken up, allowing a homogeneous distribution of the particles on the support. The annealing step of the synthesis can be performed by adding dioctylether after evaporation of the THF and treating the deposited particles at 250 °C.

Figure 7 shows TEM images of the deposited particles after reduction and annealing. The intermetallic compounds are deposited as small agglomerates on the Al_2O_3. The Pd content of the materials as determined by chemical analyses is 55 ppm and 123 ppm for $GaPd_2@Al_2O_3$ and $GaPd@Al_2O_3$, respectively.

Catalytic Performance of the Nanoparticles. Figures 8 and 9 show the conversion of acetylene during the reaction over unsupported and deposited nanoparticles of $GaPd_2$ and GaPd in comparison with ground bulk material and a commercial 5 wt.-% Pd/Al_2O_3. Pd shows a strong deactivation (more than 50% loss) within 20 h, which is typical for this catalyst. This is caused by the

dx.doi.org/10.1021/ja202869d | J. Am. Chem. Soc. 2011, 133, 9112–9118

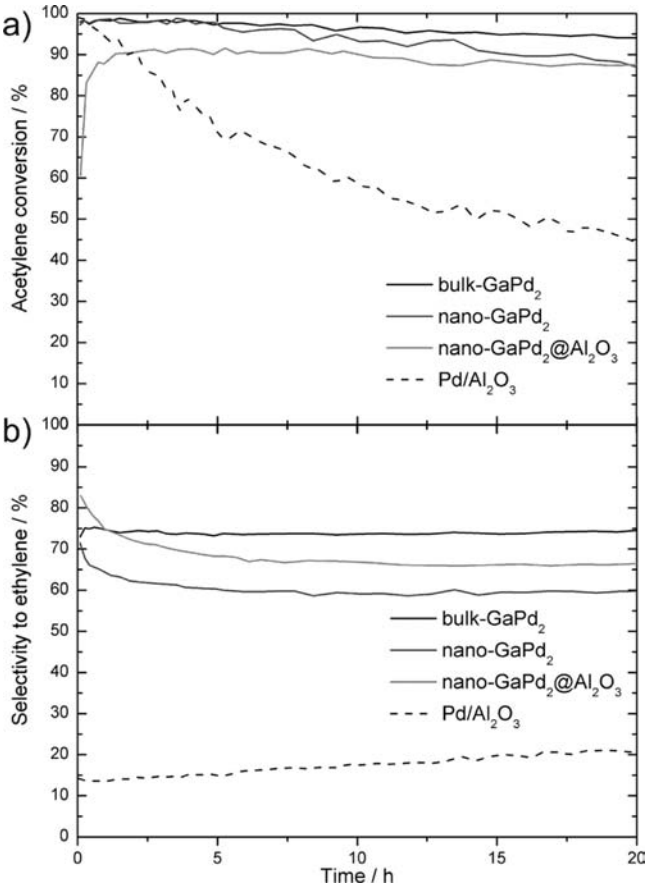

Figure 8. Comparison of (a) conversion and (b) selectivity to ethylene of bulk $GaPd_2$ (10 mg), unsupported nanoparticulate $GaPd_2$ (0.1 mg) and nanoparticulate $GaPd_2@Al_2O_3$ (100 mg). In contrast to a commercial 5% Pd/Al_2O_3 (0.15 mg), the intermetallic compounds exhibit a high long-time stability and excellent selectivities for the semihydrogenation of acetylene.

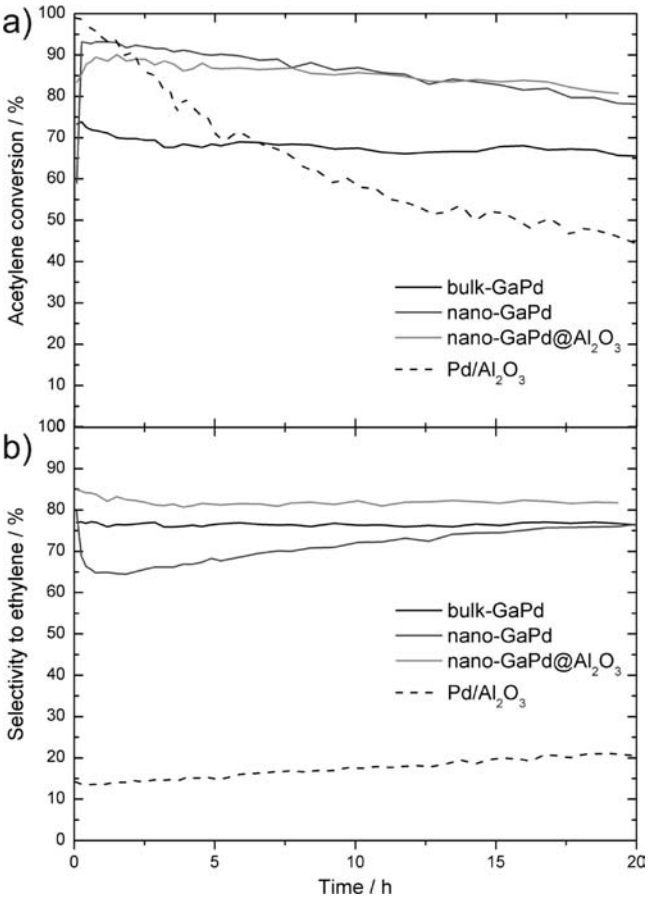

Figure 9. Catalytic properties, (a) conversion and (b) selectivity to ethylene, of bulk GaPd (400 mg), unsupported nanoparticulate GaPd (2.5 mg) and nanoparticulate $GaPd@Al_2O_3$ (75 mg) in comparison to 5% Pd/Al_2O_3. While the stability of all intermetallic compounds is similar, the selectivity of supported GaPd nanoparticles even exceeds the high selectivity of bulk GaPd.

low selectivity of Pd leading not only to ethylene or ethane but also to carbon and various oligomers which quickly deposit on the Pd surface.[3] The ground bulk-materials of GaPd and $GaPd_2$ show no deactivation during 20 h.[26] The reason for the high stability is the high selectivity, which avoids the deposition of carbon or oligomers by the site-isolated Pd atoms and by the high *in situ* stability of the compounds.[4,5]

The nanoparticulate materials show only a slight deactivation during the reaction, which is most likely caused by sintering of the particles. $GaPd_2$ shows a slight deactivation during the first 5 h and the selectivity is about 13% lower compared with the bulk material. Nanoparticulate GaPd also deactivates with time and reaches the selectivity of bulk GaPd. The mass of unsupported intermetallic material necessary to reach >90% conversion is significantly reduced by the nanostructuring. Nanoparticulate $GaPd_2$ shows a 90 times higher activity as compared to the ground bulk material, while the activity of nanoparticulate GaPd is enhanced by a factor of more than 180. Table 1 summarizes the activity of the different catalysts. By depositing the nanoparticles on the support, the activity could be significantly further enhanced, which is expected since the particles are finely dispersed on the support, reducing agglomeration and resulting in a higher accessible active surface area.

The situation is somewhat different when the activity per surface area for the different materials is compared. Here, the activity of the nanoparticulate GaPd materials is about 1 order of magnitude higher compared to bulk-GaPd, which most likely can be assigned to the higher surface curvature of the nanoparticles. In line with this is the slightly stronger deactivation with time of the nanoparticulate GaPd as well as the increase of the selectivity, which corresponds to a structural healing of the material. Deposition of nanoparticulate GaPd on Al_2O_3 results in higher stability and selectivity, which could be a consequence of the higher annealing temperature of 250 °C, leading to a more ordered surface. Bulk-$GaPd_2$, on the other hand, shows a specific activity that is about 1 order of magnitude higher than for the nanostructured materials. This counterintuitive phenomenon can either be caused by structural or electronic variations, and further investigations are in progress.

In summary, we could show that the selectivity and stability of the intermetallic compounds in a nanoparticulate state—also in presence of a support—are only slightly affected in comparison to the ground bulk materials, but the specific activity per mass is significantly enhanced. An increase by a factor 90 and more than 180 for $GaPd_2$ and GaPd, respectively, could be obtained for the unsupported particles. Deposition of the particles results in an activity increase by a factor of nearly 35 000 for GaPd and 1 300 in the case of $GaPd_2$ compared to the ground bulk material.

dx.doi.org/10.1021/ja202869d | *J. Am. Chem. Soc.* 2011, 133, 9112–9118

Table 1. Catalytic Activities of Ga−Pd Catalysts in Comparison to 5% Pd/Al_2O_3

catalyst	n_{Pd}/mmol	conversion/%	activity/$mol_{acetylene}$ $(mol_{Pd}\cdot h)^{-1}$	activity/$mol_{acetylene}$ $(a_{metal}\cdot h)^{-1}$
bulk-GaPd	2.27	65.5	1.21×10^{-1}	8.49×10^{-3}
nano-GaPd	1.42×10^{-2}	78.1	2.31×10^{1}	6.31×10^{-2}
nano-GaPd@Al_2O_3	8.67×10^{-5}	83.9	4.14×10^{3}	7.26×10^{-2}
bulk-$GaPd_2$	7.08×10^{-2}	94.7	5.44	1.93
nano-$GaPd_2$	7.08×10^{-4}	86.5	5.03×10^{2}	2.89×10^{-1}
nano-$GaPd_2$@Al_2O_3	5.17×10^{-5}	87.6	7.12×10^{3}	2.99×10^{-1}
5% Pd/Al_2O_3	7.05×10^{-5}	44.9	2.45×10^{3}	2.06×10^{-1}

CONCLUSION

In this work, the first synthetic route to single-phase nanoparticulate $GaPd_2$ and GaPd is developed. Two steps are necessary: the first step includes the coreduction of the ionic precursors by Superhydride in THF. Annealing the particles in dioctylether at 185 °C in a second step leads to a complete diffusion of Ga into Pd and gives the desired intermetallic compounds. The resulting agglomerated spherical particles have a relatively small size distribution with a maximum of 3 nm for GaPd and 7 nm for $GaPd_2$.

The reaction parameters are crucial for the success of the reaction, and the mechanism involved is not as simple as might be assumed. The reduction of Ga^{3+} is not quantitative and is mediated by elemental Pd during the first step when THF is used as solvent. Stable complexes due to the high Lewis-acidity inhibit the reduction of Ga^{3+} by $LiHBEt_3$ in absence of Pd in THF. The formation of elemental Ga at the surface of Pd seems to be an important requirement for the success of the reaction and allows the formation of intermetallic nanoparticles with homogeneous composition.

The catalytic properties are nearly maintained when compared to the ground bulk material. Nanoparticulate GaPd and $GaPd_2$ show a high selectivity (77 and 60%) and a good long-time stability for the semihydrogenation of acetylene. The overall activity in comparison with ground bulk material is enhanced by a factor of 90 in the case of $GaPd_2$ and more than 180 in the case of GaPd. The nanoparticles could be successfully deposited on Al_2O_3, leading to slightly higher selectivities and to much higher activities, which are enhanced by a factor of 1 300 in the case of $GaPd_2$ and 35 000 in the case of GaPd. On the basis of the total Pd content, the materials possess activities comparable to a commercial Pd/Al_2O_3 catalyst, while outperforming its selectivity.

This work presents a successful strategy for the development of a novel catalyst: Starting from a model catalyst system using a knowledge-based approach and taking into account fundamental aspects, it was possible to gradually create a high performance catalyst. This alternative way of catalyst development demonstrates the superiority and relevance of the intermetallic compounds in selective hydrogenation catalysis as well as their potential for industrial applications.

AUTHOR INFORMATION

Corresponding Author

*Max-Planck-Institut für Chemische Physik fester Stoffe, Nöthnitzer Strasse 40, 01187 Dresden, Germany, e-mail: Marc.Armbruester@cpfs.mpg.de.

ACKNOWLEDGMENT

We thank H. Lichte and F. Röder from the Triebenberg Laboratory for TEM measurement time. Discussions with B. Wrackmeyer, Yu. Grin as well as R. Schlögl on the underlying processes proved very valuable.

REFERENCES

(1) Arnold, H.; Döbert, F.; Gaube, J. In *Handbook of Heterogeneous Catalysis*; Ertl, G., Knözinger, H., Weitkamp, J., Eds.; VCH: Weinheim, 2008; p 3282.
(2) Johnson, M. M.; Walker, D. W.; Nowack, G. P. US Patent 4404124, 1983.
(3) Borodzinski, A.; Bond, G. C. *Catal. Rev.* **2006**, *48*, 91.
(4) Osswald, J.; Giedigkeit, R.; Jentoft, R. E.; Armbrüster, M.; Girgsdies, F.; Kovnir, K.; Ressler, T.; Grin, Yu.; Schlögl, R. *J. Catal.* **2008**, *258*, 210.
(5) Osswald, J.; Kovnir, K.; Armbrüster, M.; Giedigkeit, R.; Jentoft, R. E.; Wild, U.; Grin, Yu.; Schlögl, R. *J. Catal.* **2008**, *258*, 219.
(6) Armbrüster, M.; Kovnir, K.; Behrens, M.; Teschner, D.; Grin, Yu.; Schlögl, R. *J. Am. Chem. Soc.* **2010**, *132*, 14745.
(7) Abraham, I.; Aleandri, L. E.; Bogdanovic, B.; Kolb, U.; Lagarden, M.; Schlichte, K. *Eur. J. Inorg. Chem.* **1998**, 1699.
(8) Cokoja, M.; Jagirdar, B. R.; Parala, H.; Birkner, A.; Fischer, R. A. *Eur. J. Inorg. Chem.* **2008**, 3330.
(9) Komatsu, T.; Inaba, K.; Uezono, T.; Onda, A.; Yashima, T. *Appl. Catal.* **2003**, *251*, 315.
(10) Penner, S.; Lorenz, H.; Jochum, W.; Stöger-Pollach, M.; Wang, D.; Rameshan, C.; Klötzer, B. *Appl. Catal.* **2009**, *358*, 193.
(11) Basit, L.; Wang, C.; Jenkins, C. A.; Balke, B.; Ksenofontov, V.; Fecher, G. H.; Felser, C.; Mugnaioli, E.; Kolb, U.; Nepijko, S. A.; Schönhense, G.; Klimenkov, M. *J. Phys. D: Appl. Phys.* **2009**, *42*, 084018.
(12) Musaev, O. R.; Midgley, A. E.; Muthu, D. V. S.; Wrobel, J. M.; Kruger, M. B. *Mater. Lett.* **2009**, *63*, 893.
(13) Cable, R. E.; Schaak, R. E. *Chem. Mater.* **2005**, *17*, 6835.
(14) Chou, N. H.; Schaak, R. E. *J. Am. Chem. Soc.* **2007**, *129*, 7339.
(15) Bauer, J. C.; Chen, X.; Liu, Q.; Phan, T. H.; Schaak, R. E. *Chem. Mater.* **2008**, *18*, 275.
(16) Green, M. *Chem. Commun.* **2005**, 3002.
(17) Cable, R. E.; Schaak, R. E. *Chem. Mater.* **2007**, *19*, 4098.
(18) Astrov, D. N.; Razhba, N. A.; Razhba, Y. E. *Meas. Tech.* **1987**, *30*, 27.
(19) Friedrich, M.; Armbrüster, M. *Chem. Mater.* **2009**, *21*, 5886.
(20) Jia, C. L.; Lentzen, M.; Urban, K. *Science* **2003**, *299*, 870.
(21) Lentzen, M. *Microscopy Microanal.* **2006**, *12*, 191.
(22) Bönnemann, H.; Brijoux, W.; Joussen, T. *Angew. Chem.* **1990**, *102*, 324.
(23) Brown, H. C.; Khuri, A.; Krishnamurthy, S. *J. Am. Chem. Soc.* **1977**, *99*, 6237.
(24) Scholz, S.; Lerner, H. W.; Bolte, M. *Acta Cryst. E* **2002**, *58*, 586.
(25) Schmidt, E. S.; Schier, A.; Mitzel, N. W.; Schmidbaur, H. Z. *Naturforsch. B* **2001**, *56*, 337.
(26) Borodzinski, A.; Janko, A. *React. Kinet. Catal. Lett.* **1977**, *7*, 163.
(27) Patterson, A. L. *Phys. Rev.* **1939**, *56*, 978.
(28) Kovnir, K.; Armbrüster, M.; Teschner, D.; Venkov, T. V.; Szentmiklósi, L.; Jentoft, F. C.; Knop-Gericke, A.; Grin, Yu.; Schlögl, R. *Surf. Sci.* **2009**, *603*, 1784.